# The Entropies of Adsorbed Molecules

Charles T. Campbell* and Jason R. V. Sellers

Department of Chemistry, University of Washington, Seattle, Washington 98195-1700, United States

ABSTRACT: Adsorbed molecules are involved in many reactions on solid surface that are of great technological importance. As such, there has been tremendous effort worldwide to learn how to predict reaction rates and equilibrium constants for reactions involving adsorbed molecules. Theoretical calculation of both the rate and equilibrium constants for such reactions requires knowing the entropy and enthalpy of the adsorbed molecule. While much effort has been devoted to measuring and calculating the enthalpies of well-defined adsorbates, few measurements of the entropies of adsorbates have been reported. We present here a new way to determine the standard entropies of adsorbed molecules (S_{ad}^0) on single crystal surfaces from temperature programmed desorption data, prove its accuracy by comparison to entropies measured by equilibrium methods, and apply it to published data to extract new entropies. Most importantly, when combined with reported entropies, we find that at high coverage, they linearly track the entropy of the gas-phase molecule at the same temperature (T), such that $S_{ad}^0(T) = 0.70\ S_{gas}^0(T) - 3.3R$ (R = the gas constant), with a standard deviation of only $2R$ over a range of $50R$. These entropies, which are ~2/3 of the gas, are huge compared to most theoretical predictions. This result can be extended to reliably predict prefactors in the Arrhenius rate constant for surface reactions involving such species, as proven here for desorption.
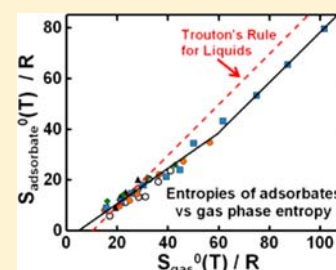
INTRODUCTION

Surface chemical reactions play a central role in many technologies that will be crucial for our energy and environmental future, including solar cells, microelectronics, computer chips, chemical and biochemical sensors, prosthetic medical devices, reflective and protective coatings, optical, electro-optic and opto-electric devices, adhesives, sorbents, solid reactants, catalysts for clean fuels and chemicals production and pollution cleanup, photocatalysts, fuel cells, and batteries. It is well established that one must know the enthalpies and entropies of the reactants if one is to develop systematic theories that can predict equilibrium and rate constants for chemical reactions of any type. While the enthalpies of adsorbates involved in surface reactions are starting to be understood, our knowledge of the entropies of adsorbates is very poor. Indeed, we know of no previous systematic studies of how the entropies of adsorbed species depend on their physical properties.

Surface chemists usually think about adsorbate entropies in terms of the two limiting cases that have been discussed in statistical thermodynamics texts: the 2D lattice and the 2D ideal gas models.[1] In calculating rate constants for surface reactions based on quantum mechanical calculations (mainly density functional theory, DFT) of reactant and transition-state (TS) energies, surface chemists almost exclusively rely on harmonic TS theory approaches, which assume that each adsorbate is a localized oscillator with only vibrational modes. Vibrations generally have very low entropy compared to translations and rotations of their gas-phase analogues. We show here that these common approximations greatly underestimate the entropies of adsorbed molecules even when they are held together in islands by attractive interactions. Instead, their entropies are almost two-thirds of the entropy of their gas-phase analogue (at temperatures high enough to measure desorption rates or

adsorption ⇌ desorption equilibria), suggesting that all components of motions in two out of the three dimensions are nearly as labile as in the gas phase. We further show that the correlation we have discovered here between the entropies of adsorbed and gas-phase molecules can be quite useful in predicting rate constants for adsorbed molecules.

EXPERIMENTAL AND THEORETICAL METHODS

While writing a review of the energetics of adsorption on single crystalline oxide surfaces recently, we also collected data for the standard entropies of adsorption (ΔS_{ad}^0 where the superscript 0 refers to the standard pressure of 1 bar) that had been experimentally measured,[2] which were rather few. All of these had been measured at high coverages by the volumetric equilibrium adsorption isotherm (EAI) method on MgO(100) smoke (a powder consisting of tiny cubes terminated in (100) faces). We calculated the standard entropies of these adsorbates at the measurement temperature, T, by simply adding the entropy of the gas at T: $S_{ad}^0 = S_{gas}^0 + \Delta S_{ad}^0$. The values of S_{gas}^0 for these molecules were found in standard thermodynamic tables and, when necessary, extrapolated to different temperatures using tabulated heat capacities. These values of ΔS_{ad}^0, S_{gas}^0, S_{ad}^0, and T are tabulated[2] and reproduced in Table 1. Figure 1 is a plot of S_{ad}^0 versus S_{gas}^0 for those data.

Inverse gas chromatography has also been used to determine adsorbate entropies on high-area powders, but to our knowledge it has not been applied to single crystalline surfaces (e.g., MgO(100) smoke) where the adsorbates are more well-defined, which is the focus here.

Temperature programmed desorption (TPD) has been widely used to measure activation energies for desorption (E_d) on single crystals. To extract E_d from TPD data, the surface species are always assumed to be in equilibrium, in which case the measured desorption rate is a single-valued function of coverage (θ) and temperature: $r(\theta,T)$. For the case of importance here, molecular adsorption/desorption, it is

Table 1. Adsorbate and Gas-Phase Entropies Determined by EAI and by Using the Prefactors Determined from TPD Data Analysis[a]

adsorbate	surface	T / K	β / K/s	$\log(\nu/s^{-1})$	$-\Delta S_{ad}^{0}/R$	$S_{gas}^{0}(T)/R$	$S_{ad}^{0}(T)/R$	ref
				Equilibrium Adsorption Isotherms				
methane	MgO(100)	77			11.0	16.9	5.95	3
ethane	MgO(100)	120			12.0	23.3	11.3	3
propane	MgO(100)	140			11.6	28.1	16.5	3
n-butane	MgO(100)	163			12.1	32.4	20.3	3
n-pentane	MgO(100)	185			16.8	36.2	19.4	3
neopentane	MgO(100)	200			17.1	40.9	23.8	4
n-hexane	MgO(100)	207			17.6	31.1	13.5	3
CH$_3$OH	MgO(100)	264			15.0	28.3	13.3	5
				Temperature Programmed Desorption				
CO	TiO$_2$(110)	170	0.5	14	8.81	21.8	13.0	6
NO	TiO$_2$(110)	128.5	0.5	13.5	7.77	21.0	13.2	7
CO$_2$	TiO$_2$(110)	177	2	13.6	8.16	23.3	15.2	8
methane	MgO(100)	47	0.6	13.1	6.77	15.0	8.20	9
methane	PdO(101)	143	1	14.7	10.2	19.3	9.06	10
methane	Pt(111)	63	0.6	12.1	4.41	16.1	11.7	11
methane	C(0001)	55	0.6	13.0	6.51	15.6	9.09	11
ethane	MgO(100)	75	0.6	14.9	11.1	20.9	9.76	9
ethane	Pt(111)	106	0.6	13.6	8.10	22.3	14.2	11
ethane	C(0001)	87	0.6	14.3	9.74	21.5	11.8	11
propane	MgO(100)	93	0.6	15.6	12.9	24.9	11.9	9
propane	Pt(111)	139	0.6	14.8	11.0	26.5	15.5	11
propane	C(0001)	110	0.6	14.6	10.6	25.5	14.9	11
n-butane	MgO(100)	111	0.6	15.7	13.3	27.8	14.5	9
n-butane	Pt(111)	171	0.6	14.7	10.9	31.9	21.0	11
n-butane	C(0001)	135	0.6	15.2	12.1	30.2	18.1	11
isobutane	ZnO(0001)	130	1.6	13.4	−7.96	28.2	20.3	12
n-hexane	MgO(100)	144	0.6	16.0	−14.1	36.4	22.3	9
n-hexane	Pt(111)	229	0.6	17.2	−16.8	42.8	26.0	11
n-hexane	C(0001)	179	0.6	17.7	−18.0	39.4	21.4	11
n-octane	MgO(100)	175	0.6	17.9	−18.6	46.0	27.4	9
n-octane	C(0001)	218	0.6	16.5	−15.3	50.0	34.6	11
n-decane	MgO(100)	204	0.6	19.1	−21.4	56.3	34.9	9
n-decane	C(0001)	254	0.6	17.8	−18.4	61.7	43.3	11

[a]As described in the text. Data from ref 2.

generally assumed that desorption is a first-order process, in which case the Polanyi−Wigner equation gives: $r(\theta,T) = -d\theta/dt = \nu \times \exp(-E_d(\theta)/RT) \times \theta$, where ν is the pre-exponential factor and R is the gas constant. One typically assumes that ν does not vary with coverage or temperature but that E_d does (as $E_d(\theta)$). One then finds the prefactor and $E_d(\theta)$ that best match the measured rates over a large range of coverages and temperatures. This method has been widely used. We next show how the prefactor found in this way can be used to get the adsorbate entropy, S_{ad}^{0}, at the desorption peak temperature, T_p.

When the adsorption ⇌ desorption process is reversible and the activation energy for adsorption is negligible, as it is for many cases of molecular adsorption of interest here, the TS for desorption is the molecule with its center of mass constricted to lie on a plane parallel to the surface at some distance far enough away from the surface that its interaction with the surface is negligible for any angle of rotation.[9,13] In this case, the TS is very well-defined. Its entropy ($S_{TS,des}^{0}$) is identical to that for the gas (S_{gas}^{0}) at the same temperature, except that it is missing one translational degree of freedom (the one perpendicular to the surface):

$$S_{TS,des}^{0} = S_{gas}^{0} - S_{gas,1D\text{-}trans}^{0} \tag{1}$$

The value of $S_{gas,1D\text{-}trans}^{0}$ for any gas can easily be calculated using statistical mechanics (the Sackur−Tetrode equation),[14] assuming that

each translational degree of freedom contributes one-third of the total 3D translational entropy. A useful formula for doing this is

$$S_{gas,1D\text{-}trans}^{0} = (1/3)\{S_{Ar,298K}^{0} + R \ln[(m/m_{Ar})^{3/2}(T/298K)^{5/2}]\} \tag{2}$$

where m is the molar mass of the gas, m_{Ar} is that for argon, and $S_{Ar,298K}^{0}$ is the entropy of Ar gas at 1 bar and 298 K (= 18.6R). Within TS theory,[15] the desorption prefactor is given by

$$\nu = k_B T/h \exp(\Delta S_{TS,des}^{0}/R) = k_B T/h \exp[(S_{TS,des}^{0} - S_{ad}^{0})/R] \tag{3}$$

where k_B is Boltzmann's constant and h is Planck's constant. Substitution using eq 1 gives

$$\nu = k_B T/h \exp[(S_{gas}^{0} - S_{gas,1D\text{-}trans}^{0} - S_{ad}^{0})/R] \tag{4}$$

This can be rearranged to give an expression for calculating S_{ad}^{0} from a measured value of ν:

$$S_{ad}^{0} = (S_{gas}^{0} - S_{gas,1D\text{-}trans}^{0}) - R \ln(\nu h/(k_B T)) \tag{5}$$

where all entropies are for the same average temperature as the measurement of ν (or $\sim T_p$).

We also applied eq 5 to get the entropies of a variety of reversibly adsorbed molecules on MgO(100) from their measured desorption
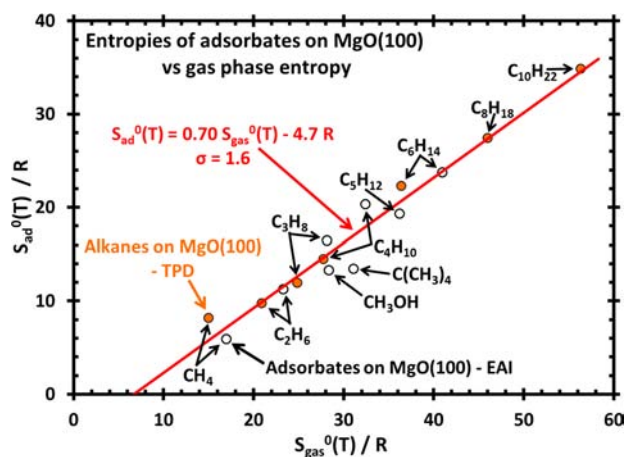
Figure 1. Plot of the standard entropies of molecular adsorbates ($S_{ad}^0 = S_{gas}^0 + \Delta S_{ad}^0$) on MgO(100) smoke determined by equilibrium adsorption isotherms (EAI), from ref 2, plotted versus the standard entropy of the gas-phase molecule at the same temperature. The standard entropies of these same and other adsorbates determined using desorption prefactors from TPD data using eq 5 are also included from ref 2. The agreement with EAI results proves the accuracy of this method. The best linear fit to these data is also shown, along with the standard deviation (σ) of the adsorbate entropies from this line.

Figure 2. Plot of the standard entropies of molecular adsorbates ($S_{ad}^0 = S_{gas}^0 + \Delta S_{ad}^0$) on MgO(100) determined by EAI and TPD, from ref 2, plotted versus the standard entropy of the gas-phase molecule at the same temperature minus the entropy for one degree of translational freedom.

prefactors as reported in the literature. The values are also tabulated along with ν, T_p and $S_{gas}^0(T_p)$ in ref 2 and reproduced in Table 1.

■ RESULTS

Figure 1 shows the standard adsorbate entropy, S_{ad}^0, for molecularly adsorbed species on the MgO(100) surface, as measured by the equilibrium adsorption isotherm (EAI) method on MgO(100) smoke (and tabulated in ref 2) and plotted versus the gas-phase entropy at the same temperature, S_{gas}^0. There is a strong, linear correlation between S_{ad}^0 and S_{gas}^0.

The entropies of a variety of reversibly adsorbed molecules on MgO(100), determined from their reported, experimentally measured desorption prefactors by using eq 5 (and tabulated in ref 2), were also added to Figure 1. The excellent agreement between the adsorbate entropies on MgO(100) obtained in this way and those directly measured by EAI verifies the accuracy of eq 5. To our knowledge, this is the first experimental verification that one can indirectly measure adsorbate entropies from TPD data for such systems. Below are its first applications, which prove quite powerful.

By combining the adsorbate entropies on MgO(100) measured by both methods in Figure 1, one can see that there is a nearly perfect linear correlation between $S_{ad}^0(T)$ and $S_{gas}^0(T)$:

$$S_{ad}^0(T) = 0.70 S_{gas}^0(T) - 4.7R \qquad (6)$$

with a correlation coefficient (R^2) of 0.96 (standard deviation = 1.6R). Note that each point here is for a different molecule (or method) at a temperature where its desorption was fast enough to perform the EAI and TPD measurements ($\sim 10^{-3}$ to 100 monolayers/s), which is the most relevant temperature for applications.

As shown in Figure 2, this linear correlation becomes a direct proportionality if we first subtract from S_{gas}^0 the entropy associated with one degree of translational freedom, $S_{gas,1D-trans}^0$. This plot is for the data on MgO(100) only, obtained by both
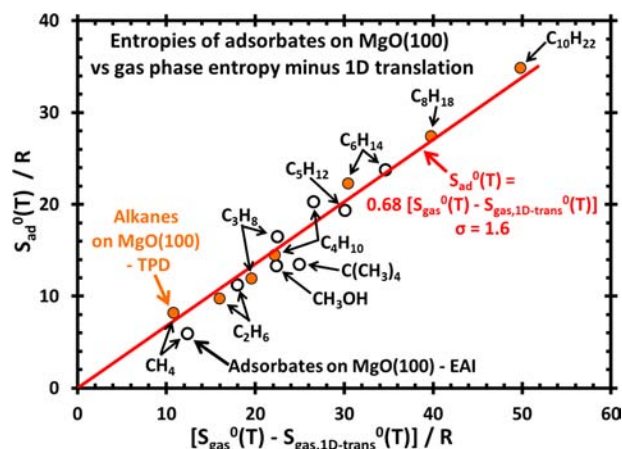
EAI and TPD. That this plot now goes through (0,0) shows that the x-intercept in Figure 1 was approximately $S_{gas,1D-trans}^0$. This much of the gas-phase entropy is totally lost in the adsorbates due to the fact that they generally sit in a potential energy well that is very steep in the direction perpendicular to the surface (z). Thus they have very restricted center-of-mass motion in z, appearing now only as a nearly negligible vibrational entropy. The proportionality constant between S_{ad}^0 and $S_{gas}^0 - S_{gas,1D-trans}^0$ is 0.68 in Figure 2:

$$S_{ad}^0 = 0.68(S_{gas}^0 - S_{gas,1D-trans}^0) \qquad (7)$$

This proportionality, which has $R^2 = 0.96$ and a standard deviation of 1.7R over a range of 40R, shows that the adsorbate maintains $\sim 2/3$ of the entropy of the gas-phase species (after subtracting the entropy of its z translation motion).

Encouraged by the excellent agreement between the entropies extracted from TPD prefactors using eq 5 and those directly measured by EAI in Figures 1 and 2, we calculated the entropies of a variety of other adsorbed molecules on single crystals from their experimentally determined desorption prefactors. This includes all the prefactors we could find for adsorbates on other oxide single crystal surfaces,[2] for linear alkanes on Pt(111)[11] and graphite(0001).[11,16,17] As shown in Figure 3, a very similar linear relationship between S_{ad}^0 and S_{gas}^0, as found in Figure 1 for MgO(100) alone, was found to hold when we include also the entropies for all these other molecularly adsorbed species and other types of surfaces. For the same range of data as in Figure 1 (i.e., up to $S_{gas}^0 = \sim 60R$), these measured entropies were very well fit by the line:

$$S_{ad}^0(T) = 0.70 S_{gas}^0(T) - 3.3R \qquad (8)$$

with a standard deviation of only 2.2R over a range of $\sim 50R$. Including this much larger data set shifted the y-intercept only very slightly (up by 1.4R) from the line for MgO(100) alone, and the slope stayed the same. This indicates that this linear relationship is nearly independent of the molecule and the solid material. Thus, eq 8 provides a very useful and simple method for estimating adsorption entropies for molecularly adsorbed gases on oxide surfaces when S_{gas}^0 is below $\sim 60R$. We also show below that this can be applied to estimate pre-exponential

18111

dx.doi.org/10.1021/ja3080117 | *J. Am. Chem. Soc.* 2012, 134, 18109–18115
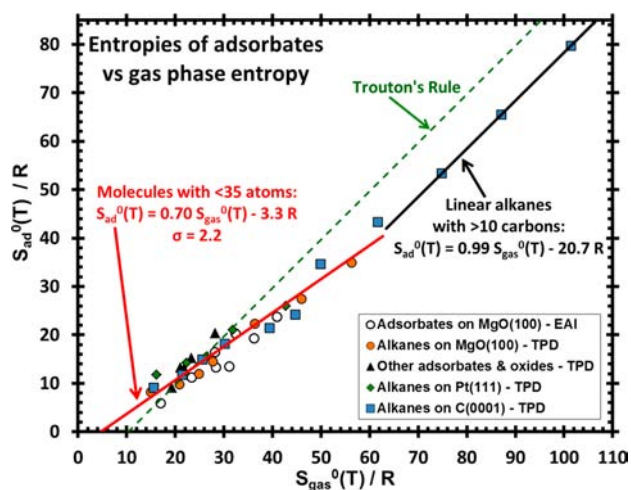
Figure 3. Plot of the standard entropies of molecular adsorbates (S_{ad}^0) on several surfaces plotted versus the standard entropy of the gas-phase molecule at the same temperature. Data for MgO(100) and other oxides are from ref 2. Entropies for linear alkanes on Pt(111) and graphite(0001) calculated using eq 5 with experimental prefactors reported in refs 9, 11, and 16. (Since the prefactor was shown to be constant between C_{12} and C_{24},[16] we used the C_{12} prefactor value for C_{14} and C_{16}.) The best linear fits to the data for molecules smaller and larger than 35 atoms are also shown. For comparison, the standard entropies of bulk 3D liquids at the normal boiling point (as estimated by Trouton's rule) are also shown.

factors in rate constants for reactions involving adsorbates, like desorption.

Table 2 shows that eq 8 is independent of the material. Here we list the slope and y-intercept values of the best-fit straight

Table 2. Parameters for Best Linear Fits to Subsets of the Data in Figure 3 Corresponding to Different Materials' Surfaces

data set	slope	standard deviation of slope	y-intercept/R	standard deviation in $S_{ad}^0(T)/R$	standard deviation in $S_{ad}^0(T)/R$ from eq 8
all points in Figure 3	0.70	0.03	−3.25	2.18	2.18
MgO(100) data only	0.70	0.04	−4.69	1.60	2.18
Pt(111) data only	0.56	0.05	−2.00	3.61	2.36
C(0001) data only	0.76	0.05	−4.42	5.01	2.34
MgO(100) EAI data only	0.72	0.10	−5.92	4.96	2.75

lines (below $S_{gas}^0 = \sim60R$) to subsets of the data in Figure 3 corresponding to the different surfaces. As seen, the slope varies from 0.56 to 0.76 between the different surfaces, but these slopes are all within two standard deviations of each other. More importantly, the standard deviation of the data for each subset about the line given by eq 8 is always less than 2.8R versus 2.18R for the full data set in Figure 3. We also show here the best-fit parameters to the EAI data alone for MgO(100).

In Figures 1 and 2, we have labeled the identities of the molecules. While most of the points are for linear alkanes, the plot includes neopentane (which is nearly spherical) and methanol (which binds specifically through its O atom to Mg

sites). Figure 3 includes all these type molecules and also points for CO, NO, CO_2, and isobutane. There are no points for large molecules on corrugated surfaces, so it is not clear if this can be generalized to highly corrugated surfaces.

The behavior is somewhat different for molecules with gas entropies above $\sim60R$, as seen in Figure 3, where the slope increased to 1.0 at high entropy (i.e., for molecules with >35 atoms). We will discuss these separately below.

◼ DISCUSSION

One possible explanation for the slope of $\sim2/3$ in Figures 1−3 is to remember that the motions of the gas molecule which give rise to most of its entropy are its translations and rotations, and these can be decomposed into their x, y, and z components. If we assume their associated entropy is equally divided between x, y, and z components, with all components of motion in the x and y directions (e.g., x and y translation and helicopter rotations) not changed from the gas, but with all components of motion in the z direction (e.g., z translation and cartwheel rotations) frozen out by the steep interaction potential well in the z direction, we arrive at a proportional relationship with slope 2/3 in Figures 1 and 3. This is certainly too simplified but captures the dominant physical effect at play here. It is consistent with a very weak corrugation of the molecule−surface interaction potential for translational and rotational motions parallel to the surface, with saddle points that are lower than RT at temperatures where desorption is fast enough to perform EAI and TPD but a steep well for any type of molecular motion perpendicular to the surface. This is similar to the model offered to explain trends in prefactors for alkane desorption.[9,11]

The weak corrugation parallel to the surface for polyatomic molecules is probably due to "lattice mismatch" between the surface's lattice constant and the bond lengths within the adsorbate: The farther the molecule extends along the surface, the bigger the fraction of its atoms not fitting in their most stable binding sites.[18] This is the same reason that the activation barrier for diffusion of a small 2D metal islands decreases with island size when the lattice mismatch with the underlying substrate is large.[19] Furthermore, within a given class of adsorbates (like alkanes), the larger the adsorbate, the larger is its adsorption energy and the hotter is T_p, so that the barrier to motions parallel to the surface could even increase in energy with size while remaining the same relative to RT_p (i.e., remain smaller than these barriers).

The entropy $S_{gas}^0 - S_{gas,1D\text{-}trans}^0$ plotted in Figure 2 is approximately $R \ln q$, where q is the partition function corresponding roughly to the number of quantum states of the gas molecule that are thermally accessible in rotational, vibrational, and 2D translational motion. The average value of $\sim25R$ in Figure 2 corresponds to $\sim10^{11}$ accessible states. The slope of 2/3 here implies that the number of accessible states drops to $\sim(10^{11})^{2/3} = \sim10^7$ after adsorption. That is a large number of states but still down by a factor of $\sim10^4$ from the gas phase.

The only case where ΔS_{ad} was measured versus coverage by EAI is for NH_3 on MgO(100) smoke, which shows a large decrease with coverage from −47 J/(mol K) (after defects are populated) to −172 J/(mol K).[20] A large decrease in ΔS_{ad} is predicted for an ideal 2D lattice gas model where adsorbate−adsorbate interactions are negligible, due to the large decrease in configurational entropy of the adsorbate as the fractional occupation of sites (θ) increases:[1]

$$S_{config} = R \ln[(1 - \theta)/\theta] \tag{9}$$

The accompanying decrease in the heat of adsorption with coverage, from 71 to 25 kJ/mol,[20] indicates that there are repulsive lateral interactions between adsorbed ammonia molecules. However, at low coverage where the average adsorbate−adsorbate separation is large, these can be neglected and the adlayer still should have very large configurational entropy, as observed. We have left the point for NH_3 off of Figure 1 since it drops from $5R$ above the line to $10R$ below the line (i.e., ∼0) with increasing coverage. Since ΔS_{ad}^0 must be defined with some "standard" coverage for a lattice gas, a standard coverage of one-half (where S_{config} drops to zero) would make it fit well. No variation with coverage was reported for the other adsorbates studied by EAI. That is, the shapes of their EAI curves were well fit by assuming that the entropy does not vary with coverage. We think this lack of coverage variation is due to the fact that they had attractive interactions and thus condensed into islands. Attractive adsorbate−adsorbate interactions are expected for these alkanes and alcohol, due to van der Waals attractions and hydrogen bonding, respectively. Since ammonia has a large dipole moment oriented perpendicular to the surface, it instead is expected to have repulsive adsorbate−adsorbate interactions, as observed. Thus, Figure 1 and eq 6 are only valid for cases with attractive interactions. A huge decrease in S_{ad} with coverage is probably characteristic of adsorbates with strong repulsive interactions.

Eq 9 brings up the question: What is the configurational entropy for those other systems that gave rise to the linear relationships of Figures 1 and 2 and eqs 6 and 7? Those were generally for cases where it appears that there are attractive adsorbate−adsorbate interactions at coverages of 1/2 ML and above, so they are clustered into 2D islands. The most common statistical mechanics model for that case is the 2D crystal lattice model and not the 2D ideal lattice gas model, which is only appropriate when there are negligible or weakly repulsive adsorbate − adsorbate interactions. There is no configurational entropy in a 2D crystal lattice, only vibrational entropy (including frustrated rotational and translational entropy). Recognizing this, it was surprising to these authors that 2/3 of the entropy associated with rotational and 2D translational motion in the gas phase still remains after adsorption. It must be that rotations and translations parallel to the surface somehow remain unhindered in such adsorbate islands. Thus, it may be more appropriate to think of these adsorbate islands at these temperatures as 2D liquids rather than as 2D crystals.

Indeed, eq 8 is similar to Trouton's Rule, which says that the standard entropy of the liquid at the normal boiling point varies approximately linearly with S_{gas}^0 with a slope of unity and a y-intercept of −10.3R.[21] For comparison, we show liquid entropies at the normal boiling point (as estimated by Trouton's Rule) in Figure 1. Adsorbate entropies drop below 3D liquid entropies only when S_{gas}^0 exceeds ∼30R, but then above ∼60R, they start tracking the liquid entropies with the same slope (within 1%), but remaining lower by a constant amount of 10.4R. Interestingly, this offset is almost exactly the same amount that liquid entropies fall below standard-state gas entropies according to Trouton's Rule (10.3R).

Although in some cases these adsorbate islands are probably in equilibrium with a low-density 2D gas phase adsorbed in the empty areas between islands (and on top of the islands), and desorption may be happening from these low-density phases,[11,22] the standard entropies we report here are for adsorbates within the dense islands themselves and not for any low-density phases that may be in equilibrium with them. This is because the measurements upon which these entropies are based tracked the dominant-species coverage in the islands and not the low density phase(s). Note too that in the derivation of TS theory, one only assumes that equilibrium is established between the reactant and the TS, and so it does not change when there are intermediate states between them.

The reason for the change in slope to 1.0 above ∼60R in Figure 3 is the same reason that the prefactors for n-alkane desorption stop increasing with chain length above 10 carbons, which has been examined thoroughly[16,17] and beautifully reproduced in molecular dynamics simulations.[18,22,23] Below C_{10}, there is a large increase in gas-phase entropy with chain length mainly due to the increasing translational entropy with mass and then the increasing moment of inertia and thus rotational entropy of these rigid-rod like molecules as they get longer. Due to the increasing probability for bends as the chains grow longer than C_{10}, the rotational entropy stops increasing above C_{10}, and the increasing entropy with chain length is now mainly due to increases in vibrational entropy. These vibrations are not effected by adsorption, so the slope goes to unity. That is, this change in slope is associated with a change in the reason that gas-phase entropies increase with molecular size: Below ∼60R, the entropy increase is mainly due to increases in translational and rotational entropy (of which ∼1/3 is lost upon adsorption), whereas above ∼60R, the gas-phase entropy increases with molecular size mainly due to increasing vibrational entropy (which is nearly unchanged upon adsorption). Since all the points above 60R in Figure 3 are for linear alkanes, it is not clear if this change in slope will be generally true. It may not appear for other classes of molecules that do not have this change from linear to nonlinear structure at a size corresponding to ∼60R.

The adsorbate entropies plotted here are huge compared to most prior models for adsorbates. In particular, the harmonic approximation, which is very widely applied to DFT calculations of adsorbate energies to estimate their rate constants, is only valid at low temperatures, but it dramatically underestimates their entropies at the temperatures of Figures 1−3 where desorption rates and equilibria are measured. This is not because the second derivatives of energy versus distance at the energy minima are incorrect (as that would lead to much smaller errors) but instead due to the low energies of the next maxima in the potential energy surface (relative to RT). This is the same reason that the hindered rotation of one methyl group about the C−C axis in gas-phase ethane contributes only low vibrational entropy at low temperature, but when RT exceeds the barrier for that methyl rotation, that mode becomes a free rotor; and when RT is only 15% of the barrier, there is already a very large increase in entropy.[14] The large error of the harmonic approximation in estimating prefactors was recently pointed out for propane desorption from PdO(101).[24]

Note that the conclusion of eq 8, that the adsorbate entropy is a large fraction of the gas-phase entropy, is qualitatively consistent with the findings of Santiago et al.[25] They approximated the entropy of an adsorbed species as a fraction F_{loc} of the gas-phase entropy minus that for its three translational components, $S_{ad}^0 = F_{loc} (S_{gas}^0 - S_{gas,3D-trans}^0)$, where F_{loc} is the fraction of the nontranslational entropy that is preserved upon adsorption. By fitting a microkinetic model to kinetic data for the selective reduction of acetic acid, methyl acetate, and ethyl acetate over silica-supported copper catalysts,

they found F_{loc} to be very large, between 0.91 and 1.00. Three later studies also found large values near 0.95 for other adsorbates on metal catalysts using similar fitting methods, as reviewed by Goldsmith.[26]

We next show that one can use the entropy correlation of Figure 1 (eq 8) to make reliable estimates of prefactors in rate constants for adsorbate reactions using TS theory. We demonstrate this for the simplest case: desorption after nonactivated molecular adsorption with attractive adsorbate–adsorbate interactions. Substituting eq 8 into eq 4 gives the prefactor:

$$\nu = k_B T/h \, \exp[(0.30 S_{gas}^0 + 3.3R - S_{gas,1D\text{-trans}}^0)/R]$$

$$= (k_B T/h) \exp\{0.30 S_{gas}^0/R + 3.3 - 9.31 \ln[(m/m_{Ar})(T/298 \text{ K})]\}$$

(10)

where $S_{gas,1D\text{-trans}}^0$ can be calculated from eq 2. Figure 4 shows a plot of the predictions of eq 10 plotted versus experimentally
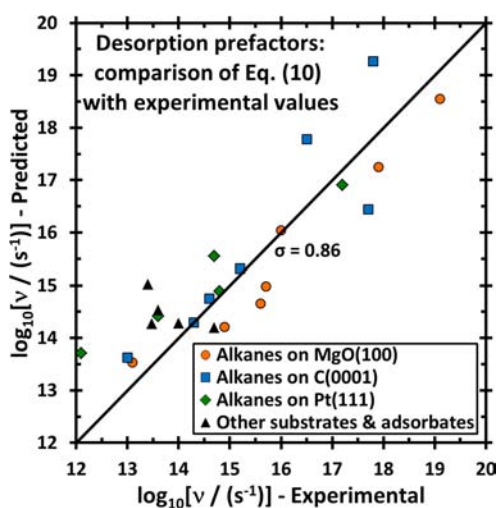
Figure 4. Prefactors for the desorption of molecularly adsorbed species as predicted from the gas-phase entropies using eq 10 (which was derived from the linear relationship in Figure 3 using TS theory) plotted versus the experimentally measured prefactors. Data are for various molecules on oxide single crystals from ref 2 and for *n*-alkanes on graphite(0001) and Pt(111) from ref 11. The line shows the expectation based on eq 10, which the data fit with a standard deviation in $\log(\nu/s^{-1})$ of 0.86.

measured desorption prefactors for all the molecules on single crystals surfaces in Figure 1 except alkanes longer than C_{10}. The predictions agree very well with these experimental prefactors with a standard deviation in $\log(\nu/s^{-1})$ of only 0.86, confirming the validity of eq 10 for estimating prefactors. For alkanes longer than C_{10}, the prefactor stays constant at $\sim 10^{19}$ s^{-1}.[16,17] Several discussions of the values for desorption prefactors have been published, but none of these have presented any relationships with prediction integrity anywhere near as good as eq 10.[9,11,16–18,22,23,27–34] Using twice the standard deviation on $\log(\nu/s^{-1})$ of 0.86 in Figure 4 gives a factor of 50 maximum error in ν at the 95% confidence limits. This analysis corresponds to terrace sites. We are not confident in the accuracy of its application to defect sites, since we have shown previously that metal adatoms have a desorption prefactor that is 10^5-fold larger at step edges than at terrace sites on Mo(100),

due to the loss of all translational motion except in the one direction along the step edge.[33]

While this potential error in rate constant seems terrible, it marks a huge improvement over the current state. There are two dominant applications of estimated prefactors. The most important is in using adsorbate and TS energies calculated with DFT together with prefactors (estimated using the second derivative of energy with coordinates and the harmonic approximation) to estimate rates of elementary steps in catalysis, and from this to propagate rates from microkinetic models of catalytic reactions.[35–39] As noted above, the harmonic approximation is much worse. The second use of prefactors is in extracting desorption energies from TPD data. Here, the maximum error in ν of 50 corresponding to a maximum error in the desorption energy of only $4.0 RT_p$ (<10 kJ/mol when $T_p = 300$ K).

Note that eq 10 is based on Figure 3's experimental correlation between adsorbate and gas-phase entropies (i.e., eq 8). Since most of the entropies plotted in Figure 3 come from the same prefactors as plotted in Figure 4, it is thus not surprising that eq 10 fits the prefactors in Figure 4 rather well. However, many of the points in Figure 3 are from entropies that were instead directly determined by EAI and not from prefactors. More importantly, Figure 3 shows that EAI entropies (when plotted alone) are well fitted by eq 8, and Table 2 shows that a fit to the EAI data alone gives a very similar slope and y-intercept. Thus, a line with a very similar slope and y-intercept to eq 10 in Figure 4 would also result if we had not used any of the entropies determined from prefactors to get eqs 8 and 10 and instead used only EAI entropies.

■ CONCLUSIONS

We have shown that the standard-state entropies of molecularly adsorbed species which have attractive adsorbate–adsorbate interactions are large and track their corresponding gas-phase entropies as $S_{ad}^0(T) = 0.70 \times S_{gas}^0(T) - 3.3R$ up to $S_{gas}^0(T) = 60R$. This relationship applies at temperatures where desorption rates are fast enough to perform EAI and TPD measurements ($\sim 10^{-3}$ to 100 ML/s). It provides an important tool to aid in estimating equilibrium constants and rate constants for reactions where these adsorbates are reactants, as proven here for desorption rate prefactors. For longer adsorbed molecules where $S_{gas}^0(T)$ exceeds 60 K (e.g., linear alkanes with >11 carbons), their entropies remain a constant 20.7R below gas entropies and $\sim 10.4R$ below Trouton's rule for liquid entropies.

■ AUTHOR INFORMATION

Corresponding Author

campbell@chem.washingon.edu

Notes

The authors declare no competing financial interest.

■ REFERENCES

(1) Hill, T. L. *An Introduction to Statistical Thermodynamics*; Addison-Wesley: Reading, MA, 1960.

(2) Campbell, C. T.; Sellers, J. R. V. *Chemical Reviews*; submitted.

(3) Arnold, T.; Cook, R. E.; Chanaa, S.; Clarke, S. M.; Farinelli, M.; Yaron, P.; Larese, J. Z. *Phys. B: Condens. Matter* **2006**, *385*, 205.

(4) Trabelsi, M.; Saidi, S.; Chefi, C.; Picaud, S.; Hoang, P. N. M.; Coulomb, J. P. *Surf. Sci.* **2004**, *550*, 133.

(5) Trabelsi, M.; Saidi, S.; Chefi, C.; Martin, C.; Lucas, S.; Ferry, D.; Suzanne, J. *Surf. Sci.* **2004**, *566*, 789.

(6) Linsebigler, A.; Lu, G. Q.; Yates, J. T. *J. Chem. Phys.* **1995**, *103*, 9438.

(7) Sorescu, D. C.; Rusu, C. N.; Yates, J. T. *J. Phys. Chem. B* **2000**, *104*, 4408.

(8) Thompson, T. L.; Diwald, O.; Yates, J. T. *J. Phys. Chem. B* **2003**, *107*, 11700.

(9) Tait, S. L.; Dohnalek, Z.; Campbell, C. T.; Kay, B. D. *J. Chem. Phys.* **2005**, *122*, 164708.

(10) Weaver, J. F.; Hakanoglu, C.; Hawkins, J. M.; Asthagiri, A. *J. Chem. Phys.* **2010**, *132*, 024709.

(11) Tait, S. L.; Dohnalek, Z.; Campbell, C. T.; Kay, B. D. *J. Chem. Phys.* **2006**, *125*, 234308.

(12) Wang, J.; Hokkanen, B.; Burghaus, U. *Surf. Sci.* **2006**, *600*, 4855.

(13) Fichthorn, K. A.; Miron, R. A. *Phys. Rev. Lett.* **2002**, *89*, 196103.

(14) McQuarrie, D. A. *Statistical Mechanics*; University Science Books: Sausalito, CA, 2000.

(15) Atkins, P. *Physical Chemistry*; 6th ed.; W. H. Freeman & Company: New York, 1998.

(16) Paserba, K. R.; Gellman, A. J. *J. Chem. Phys.* **2001**, *115*, 6737.

(17) Gellman, A. J.; Paserba, K. R. *J. Phys. Chem. B* **2002**, *106*, 13231.

(18) Becker, K. E.; Fichthorn, K. A. *J. Chem. Phys.* **2006**, *125*, 184706.

(19) Hamilton, J. C. *Phys. Rev. Lett.* **1996**, *77*, 885.

(20) Sidoumou, M.; Panella, V.; Suuzanne, J. *J. Chem. Phys.* **1994**, *101*, 6338.

(21) Atkins, P. *Physical Chemistry*; 6th ed.; W. H. Freeman & Company: New York, 1997.

(22) Becker, K. E.; Mignogna, M. H.; Fichthorn, K. A. *Phys. Rev. Lett.* **2009**, *102*, 046101.

(23) Fichthorn, K. A.; Becker, K. E.; Miron, R. A. *Catal. Today* **2007**, *123*, 71.

(24) Antony, A.; Asthagiri, A.; Weaver, J. F. *Phys. Chem. Chem. Phys.* **2012**, *14*, 12202.

(25) Santiago, M. A. N.; Sanchez-Castillo, M. A.; Cortright, R. D.; Dumesic, J. A. *J. Catal.* **2000**, *193*, 16.

(26) Goldsmith, C. F. *Top. Catal.* **2012**, *55*, 366.

(27) Paserba, K. R.; Vaidyanathan, N.; Gellman, A. J. *Langmuir* **2002**, *18*, 9799.

(28) Lombardo, S. J.; Bell, A. T. *Surf. Sci. Rep.* **1991**, *13*, 1.

(29) Madix, R. J.; Ertl, G.; Christmann, K. *Chem. Phys. Lett.* **1979**, *62*, 38.

(30) Sellers, H.; Gislason, J. *Surf. Sci.* **1999**, *426*, 147.

(31) Wise, M. L.; Koehler, B. G.; Gupta, P.; Coon, P. A.; George, S. M. *Surf. Sci.* **1991**, *258*, 166.

(32) Zhdanov, V. P. *Surf. Sci. Rep.* **1991**, *12*, 183.

(33) Starr, D. E.; Campbell, C. T. *J. Am. Chem. Soc.* **2008**, *130*, 7321.

(34) Campbell, C. T.; Sun, Y.-K.; Weinberg, W. H. *Chem. Phys. Lett.* **1991**, *179*, 53.

(35) Reuter, K.; Frenkel, D.; Scheffler, M. *Phys. Rev. Lett.* **2004**, *93*, 116105.

(36) Campbell, C. T. *Nature* **2004**, *432*, 282.

(37) Honkala, K.; Hellman, A.; Remediakis, I. N.; Logadottir, A.; Carlsson, A.; Dahl, S.; Christensen, C. H.; Norskov, J. K. *Science* **2005**, *307*, 555.

(38) Reuter, K.; Scheffler, M. *Phys. Rev. B* **2006**, *73*, 045433.

(39) Gokhale, A. A.; Dumesic, J. A.; Mavrikakis, M. *J. Am. Chem. Soc.* **2008**, *130*, 1402.